ICAT 2002
December 4-6, Tokyo, Japan

# Toward Automatic Construction of Reality-based Virtual Space Simulator

**Hiromi T.Tanaka*1, Kiyotaka Kushihama*1 and Shin-ichi Hirai*2**

*1**Computer Vision Laboratory Computer Science Dept. Ritsumeikan University**
*2**Robotics Department Ritsumeikan University**
*hiromi, kiyotaka@cv.cs.ritsumei.ac.jp*

## Abstract

Real-world objects exhibit rich physical interaction behaviours on contact. Such behaviours depend on how heavy and hard it is when hold, how its surface feels when touched, how it deforms on contact, etc. Recently, there are thus growing needs for haptic exploration to estimate and extract such physical object properties as mass, friction, elasticity, relational constraints etc.. In this paper, we propose a novel paradigm, we call haptic vision, which is a vision-based haptic exploration approach toward an automatic construction of reality-based virtual space simulator, by augmenting active vision with active touch. We apply this technique to mass, elasticity and relational constraints estimation, and use these results to construct virtual object manipulation simulator. Experimental results show that feasibility and validity of the proposed approach.

## 1. Introduction

Recently, haptic interface has been intensively studied ([2]-[4]) for providing a sense of touch in virtual environments, which is an essential modality to explore, recognize and understand the real world. Real-world objects exhibit rich physical interaction behaviours on contact. Such behaviours depend on how heavy and hard it is when hold, how its surface feels when touched, how it deforms on contact, and how it moves when pushed, etc. These aspects of visual and haptic behaviour provide important interaction cues for manipulating and recognizing objects in virtual environments. There are thus growing needs for haptic exploration to estimate and extract physical object properties such as mass, friction, elasticity, relational constraints etc.

Thus, we ahve proposed a novel paradigm, we call haptic vision, which is a vision-based haptic exploration approach toward an automatic construction of reality-based virtual space simulator. As Figure 1 shows, Haptic vision is an augmentation of active vision with active touch, which designs and controls a contact to an object so that object's behaviours are caused most effectively, based on 3D shape and posture analysis by active vision. Physical object properties are then estimated through motion analysis on real-time range and color images observing object's behaviours against a known contact.

The work on physical object properties from interaction with robots had first introduced in the early 1980 [1]. While recent progress in haptic exploration with dextrous robot hands([2]-[6]), which requires complex robot control and grasping technique, we believe this is the first non-contact vision-based automatic approach for haptic exploration to model both geometrical and physical properties of real-world objects.

We apply this technique to mass, elasticity, and relational constraints ([11]) estimation, and use these results to construct virtual object manipulation simulator. Experimental results show that feasibility and validity of the proposed approach.

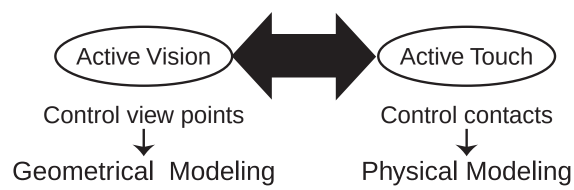


Fig. 1: Haptic Vision

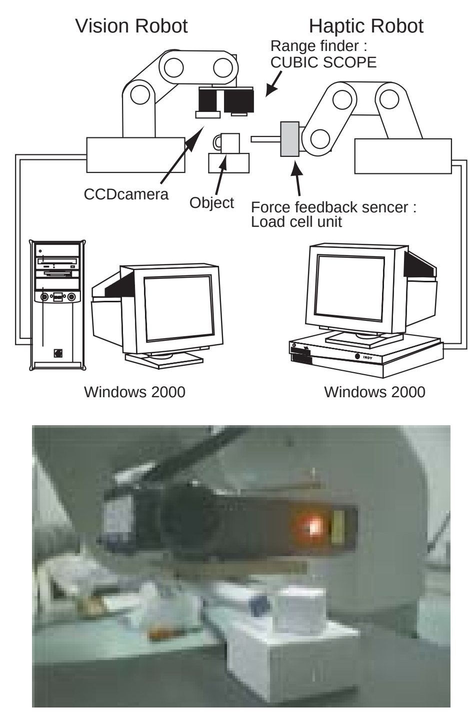


Fig. 2: Haptic Vision System

## 2. Haptic Vision

Haptic vision paradigm is motivated by recent development of a real-time handy laser range finder [8] which provides a func-

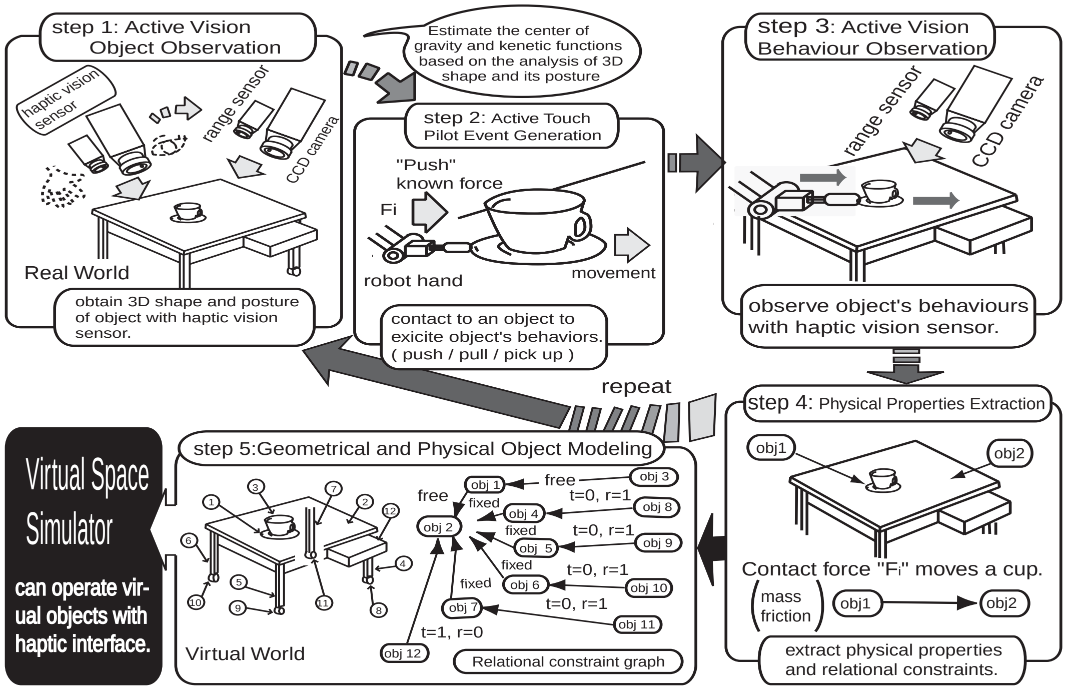


Fig. 3: Haptic Vision Approach

tion equivalent to human tactile sensing. That is, it acquires both static and dynamic geometrical information, i.e., it acquires 3D shape and deformation from real-time images, without contacting to the object and thus without dextrous robot hands.

Figure 2 shows our haptic vision system. Our haptic vision sensor, mounted on a robot hand, consists of a CCD camera and a real-time range finder where a CCD camera plays a roll of an ”eye” to obtain a wide view of the scene, and a real-time range finder plays a roll of a ”hand” to obtain 3D geometrical information by exploring surfaces of objects within a reach of a human hand. The other robot hand with a force-feed back sensor (a Load Cell Unit) makes a contact to cause object’s behaviours.

Figure 3 shows our haptic vision approach.

In step1, we first observe an object by active vision to extract and model its geometrical properties such as 3D shape, surface texture and a posture using our haptic vision sensor.

In step 2, we design and then make a contact to an object by active touch based on 3D shape and posture analysis by active vision. Such contact causes object’s behaviours most effectively and stably. We call this dynamic scene of object’s response as a pilot event where a prototypical behaviour due to the objective physical property is exhibited on response to a known contact force. We then estimate a next viewpoint from which the pilot event is observed most efficiently and stably, and move a haptic vision sensor to observe the pilot event by active vision, in step 3.

In step 4, physical object properties and relational constraints among objects are then estimated and extracted through motion analysis on real-time range and color images observing object’s behaviours.

In step 5, we generate a scene representation as a relational constraint graph where each node represents an object with both geometrical and physical properties, and each arc represents adjacency relation with a degree of freedom in both rotation ($0 \leq r \leq 3$) and translation ($0 \leq t \leq 3$).

Above steps are repeated for each object in the scene until the scene representation for a reality-based virtual object manipulation will be completed.

## 3. Haptic Exploration

We first observe an man-made object in an indoor scene using our active shape inferring algorithm [9]. Our active vision system automatically acquires a set of principal views as shown in Fig. 4 based on the symmetry in stable postures, which are mostly orthographic and are efficiently used for 3D shape reconstruction.

### 3.1 Estimating Mass

Our approach to mass estimation is as follows. In the current stage, we assume that both static and dynamic friction coefficients, $\mu_s$ and $\mu_d$, of an object are given.

In step 1, we first estimate the plane of symmetry $S$ passing through the center of gravity(COG), from a set of principal views acquired by our active vision system, as shown in Fig. 4.

In step 2, we design and make a contact by ”Push” operation by a robot hand, at a point $P_c$ of the intersection of its surface and $S$, with the direction of a contact force $F$ parallel to the horizontal plane and also included in the plane of symmetry, as shown in Fig. 5. Such contact force exerts on a center of friction and causes a pilot event for mass extraction where an object moves straight in the direction of $F$ with no rotation and with no change in its posture.

In step 3, we measure transition of $F$ during ”Push” contact using a force-feedback sensor mounted on a robot hand. In general, a friction force $F$ starts to increase at a contact point $t_c$, and rises up sharply until it reaches to the maximum friction $F\mu_s$ at

$t_s$, at which the objects starts to move. Then, it drops a little, and goes into a steady state at $F\mu_d$, as shown in Fig. 6. We also track an object from a top view point during contact to confirm its straight movement, as shown in Fig. 7.

In step 4, we then estimate a mass $M$ from $F\mu_s$ and $F\mu_d$ respectively as,

$$F\mu_s = \mu_s Mg \quad (1)$$
$$F\mu_d = \mu_d Mg \quad (2)$$

where $g$ is a gravity force.

Fig. 8 and Table 1 shows mass estimation results of a ceramic coffee cup on a base surface of three material types, wood, rubber, and steel, respectively. Error rates show that mass estimation with $\mu_s$ are performed with reasonable accuracy except on a rubber surface of large friction coefficient.

Since we estimate a mass from eq.(1) and (2) assuming that friction coefficients $\mu_s$ and $\mu_d$ are known, the mass estimation accuracy thus depends on the stability of $\mu_s$ and $\mu_d$ in various environments where they are measured. We first estimate both $\mu_s$ and $\mu_d$ from eq.(3) and (4) by measuring an angle $\theta$, a time $T$ and a length $L$ while an object is sliding, as shown in Fig. 9.

$$\mu_s = tan\theta \quad (3)$$
$$\mu_d = tan\theta - \frac{2L}{gt^2 cos\theta} \quad (4)$$

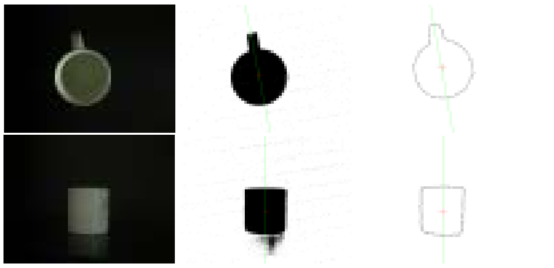

Fig. 4: Principal Views and Silhouettes of a Cup Aquired by Our Active Vision System

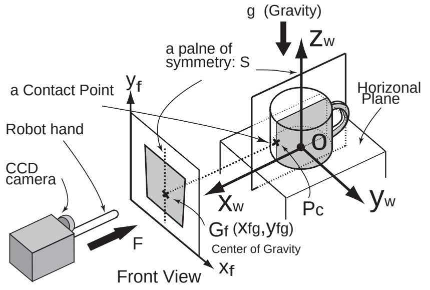


Fig. 5: Contact for Mass Estimation

We then evaluate the estimated $\mu_s$ and $\mu_d$ to confirm their stabilities against changes in both temperature and humidity. Fig. 10 and 11 show Values the measurement results of $\mu_s$ and $\mu_d$ v.s. temperature and humidity changes, respectively. The results show that $\mu_s$ is more stable than $\mu_d$. Table 2 shows the measurement of $\mu_s$ and $\mu_d$ using a sliding method as shown in Fig.

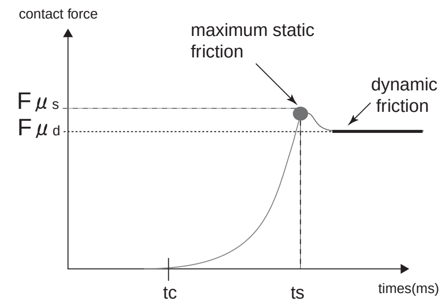


Fig. 6: Contact Force Transition Graph

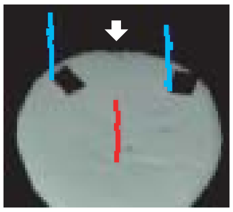

Fig. 7: Trajectory of straight movement

9. Fig. 9 Table 3 and Table 4 show the results of mass estimation on a ceramic cap, an aluminum block and a ceramic cup with craft tapes stuck on its bottom surface for static ($\mu_s$) and dynamic ($\mu_d$) friction coefficient. The stability evaluation of $\mu_s$, and $\mu_d$ in Fig. 10 and in Fig. 11,and the mass estimation results in both Table 3 and 4 show that mass estimation with $\mu_s$ is more stable, with maximum error of 7.4010%.

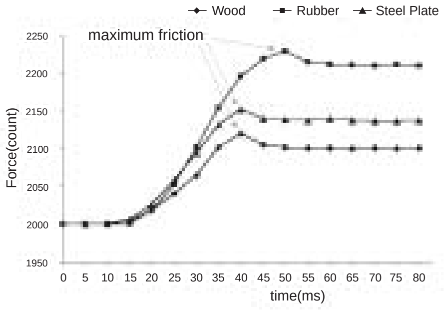


Fig. 8: Contact Force Transition for a Cup on Wood, Rubber and Steel Plate Surfaces

### 3.2 Estimating Elasticity

Our approach to elasticity estimation by "Push" is as follows. When estimating elastic coefficient of an object using Push operation of the robot hand, we have to apply a contact force that deforms the it but does not make it move nor rotate since we have to know the deformation of elastic object. So, we have to apply a contact force perpendicular to the support plane that goes through the object's the center of gravity(COG) while keeping it on the support plane in the stable posture. If we limit the candidate support plane that is taken through the scene observation to level or horizontal one, we can define the contact force as perpendicular to the object and its the direction of a contact force goes through the 2D mass center of the top view contour image.

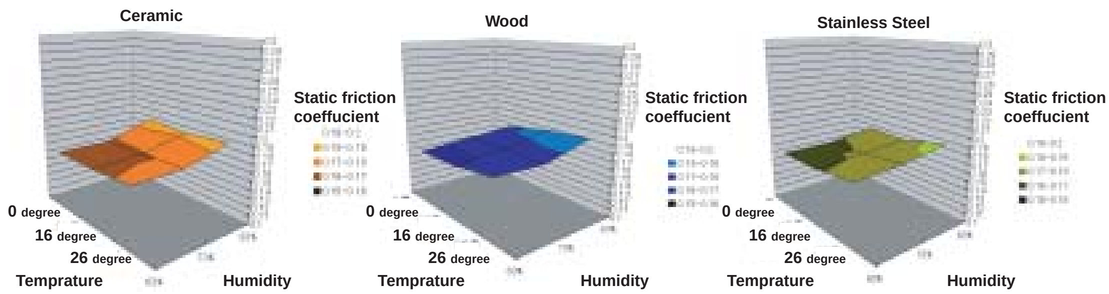


Fig. 10: Static friction coefficients V.S. temperature & humidity change

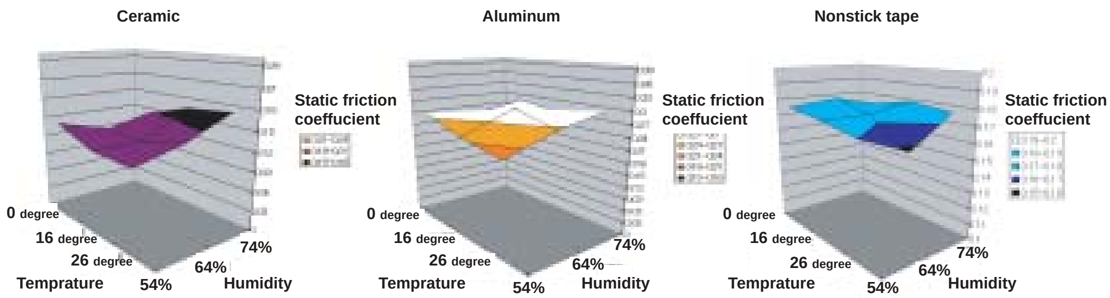


Fig. 11: Dynamic friction coefficient V.S temperature & humidity change

Table 1: Mass Estimation Results with $\mu_s$

| Base Surface | Contact Force(gw) | Static Fric. Coeff.: $\mu_s$ | Estim-ated(g) | Real (g) | Error (%) |
|---|---|---|---|---|---|
| Wood | 46.8 | 0.217 | 215.7 | 221 | 2.4 |
| Rubber | 94.9 | 0.533 | 178.0 | 221 | 19.5 |
| Steel Plate | 64.2 | 0.306 | 209.8 | 221 | 5.1 |

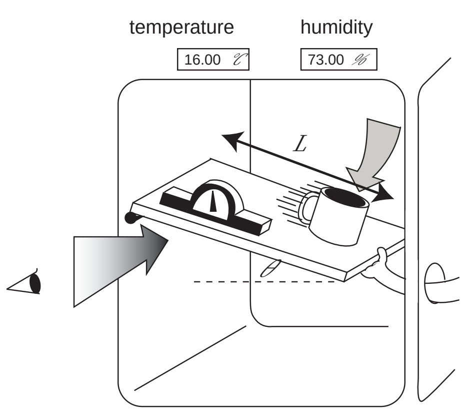


Fig. 9: Measurement of friction coefficient

Table 2: Result of friction coefficient measurement

| Base Surface (Real Mass) | Angle ($\theta$) | Time T(s) | Distance L(m) | Stasic Fric. $\mu_s$ | Dynamic Fric. $\mu_d$ |
|---|---|---|---|---|---|
| Aluminum (282g) | 15 | 14.25 | 0.38 | 0.26709 | 0.26742 |
| Ceramic (290g) | 11.8 | 9.71 | 0.4 | 0.209 | 0.203 |
| Craft tape (378g) | 11 | 73.81 | 0.4 | 0.19438 | 0.19436 |

Table 3: Mass Estimation Results with $\mu_s$

| Object | Contact Force (gw) | Static Fric. Coeff.: $\mu_s$ | Estim-ated(g) | Real (g) | Error (%) |
|---|---|---|---|---|---|
| Aluminum | 174.9 | 0.2679 | 261.09 | 282 | 7.413 |
| Ceramic | 146.2 | 0.208 | 279.92 | 290 | 3.473 |
| Craft tape | 201.7 | 0.1943 | 403.59 | 378 | 6.77 |

Table 4: Mass Estimation Results with $\mu_d$

| Object | Contact Fo-rce: $F$ (gw) | Dynamic Fr-ic. Coeff. $\mu_d$ | Estima-ted $M$ (g) | Real (g) | Error (%) |
|---|---|---|---|---|---|
| Aluminum | 175.6 | 0.2674 | 262.52 | 282 | 6.905 |
| Ceramic | 110.5 | 0.203 | 212.47 | 290 | 26.73 |
| Craft tape | 197.2 | 0.19435 | 394.79 | 378 | 4.44 |

Note that the $x_t$ and $y_t$ components of the 2D mass center of the top view contour image ($x_t$, $y_t$, $z_t$) should coincide with $x_g$ and $y_g$ components of the center of gravity ($x_g$, $y_g$, $z_g$). Thus, the elastic object to be observed should be plane symmetry and should have at least one plane of symmetry that is perpendicular to the support plane. We have adopted a cylindrical object for the elastic coefficient estimation, since cylinder is the shape that satisfies these condidions.

In step 1, Take a top view of the object by observing it from a perpendicular point. Then estimate the 2D mass center of the top view contour image and the plane of symmetry that includes the the center of gravity.

In step 2, Apply an external force to the object by the Push operation of the robot hand. The speed of the Push operation is constant and the point of contact is at the intersection $P_c$ of the object surface and a line perpendicular to the object that goes through the 2D mass center of the top view contour image $G_{top}$ estimated from the top view shown in figure 12 (a). The direction of the force is downward, that is the action line of the force goes through the contact point $P_c$ and the center of gravity that is perpendicular to the support plane.

In step 3, Apply an external force as shown in figure 13 while monitor its strength using a force feedback sensor attached onto the robot hand. Figure 13 is a graph that shows the transition of contact force when the object deforms by the external force $F$ applied to the object. The period from $t_c$ to $t_s$ corresponds to the operation gradually applying downward force by pulling the force feedback sensor down. The period from $t_s$ to $t_e$ is the waiting time in which we are waiting until the elastic oscillation calms down while keeping the pressure constant. $t_e$ is the time when the external force is removed.

In step 4, Observe the deformation using a camera and a range finder as shown in figure 12 (b). We have observed the disposition of the point $P_v$, that is the intersection of object surface and a line parallel to the support plane which goes through the 2D mass center $G_v$ of the 2D side view image, while placing the camera to the position (Pos. $P_s$) shown in figure 12 (b). What we have to know is the disposition of the point $P_v$ in the z-axis direction in the world coordinate system ($X_w$, $Y_w$, $Z_w$) shown in figure 12 (b). The disposition ($\varepsilon$) can be obtained by subtracting $H$ from $H_{init}$, where $H_{init}$ is the original height of the object before applying force and $H$ is the height observed in the image under pressure by converting the number of pixels that shows the extent of the object in $Y_v$ direction in the side view image.

$$H = \frac{110}{480}h \tag{5}$$

$$\varepsilon = |H_{init} - H| \tag{6}$$

In step 5, Estimate the elastic coefficient E from the disposition ($\varepsilon$) and force $F$ from the force feedback sensor using the following equation.

$$F = E\varepsilon \tag{7}$$

Figure 14 is a graph that shows the relation between the external force $F$ and time $t$, and between the disposition ($\varepsilon$) and time $t$ where $t_c$ is the time when the external force $F$ is started to be applied, the period from $t_s$ to $t_e$is the period of constant pressure waiting the elastic oscillation calms down and $t_e$ is the time when the external force is removed. Table 5 shows the result of experiment using two springs of different elastic coefficient. Through this experiment, we have confirmed that the elastic coefficient can be estimated stably within the error of 5 percent or so.

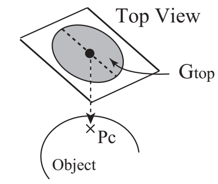


**(a) A contact point in top view**

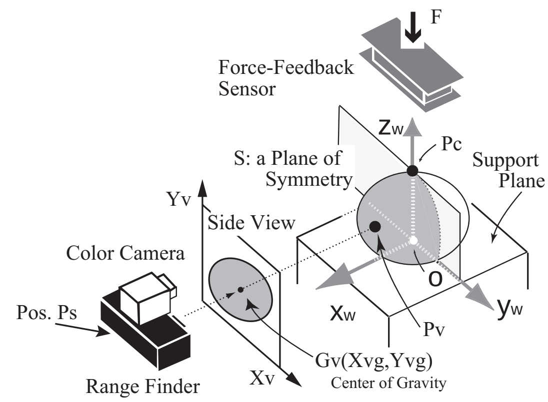


**(b) Contact for elasticity estimate**

Fig. 12: Contact for Elasticity Estimate

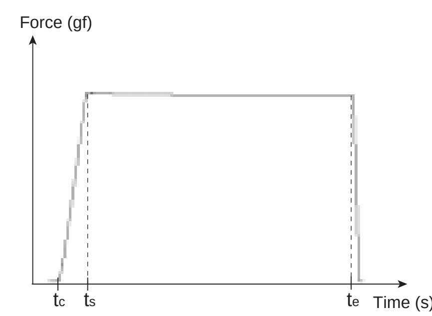


Fig. 13: Contact Force Transition Graph for Elastic Body

Table 5: Elastic Coefficients Estimation Results

| | Outside Diameter (mm) | Height (mm) | Estimated (kgf/mm) | Real (kgf/mm) | Error (%) |
|---|---|---|---|---|---|
| Spring 1 | 32.0 | 65.0 | 0.390 | 0.37 | 5.41 |
| Spring 2 | 45.0 | 80.0 | 0.794 | 0.76 | 4.57 |

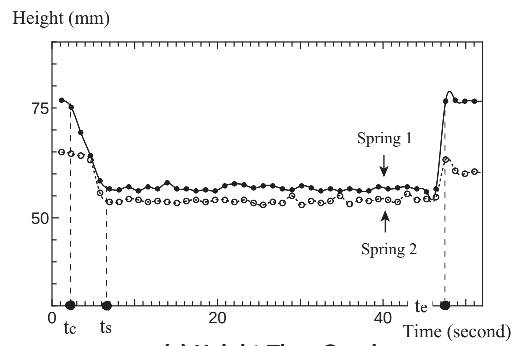


**(a) Height-Time Graph**

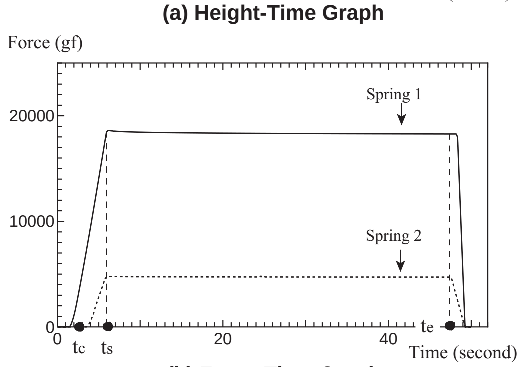


**(b) Force-Time Graph**

Fig. 14: Contact Force and Height Transition for Spring

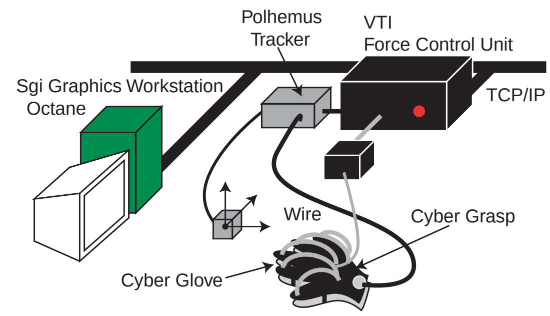


**(a) system configuration**

**(b) "Pick Up" manipulating scene**

Fig. 15: Reality-Based Virtual Object Manipulation Simulator

## 4. Reality-based Virtual Object Manipulation

We construct a virtual object manipulation simulator from a scene graph representation generated by haptic vision, with the number of objects, their 3D shape, mass, elasticity and relational constraints.[11] Figure 15 (a), (b) show a system configuration of our VR simulator and some scene of ”Pick Up” manipulation with a Cyber Glove. Given the scene graph, our ”Pick Up” simulation of the upper part causes no change in both rotation and translation of the lower part for two separate objects. Conversely the same ”Pick Up” bring up the lower part together for a single (glued) object.

## 5. Conclusion

We have proposed a haptic vision paradigm for a vision-based haptic exploration as an augmentation of active vision with active touch which causes object’s prototypical behaviours to be observed by active vision. Preliminary experimental results, on mass estimation, elasiticity estimation, relational constraints estimation, presented in companion paper [11], and automatic construction of virtual object manipulation simulator shows the feasibility and validity of the proposed approach.

## References


1. E. Krotkov, ”Perception of Material Properties by Robotic Probing: Preliminary Investigations ,” Proc. Intl. Joint Conf. Artifical Intelligence, Montreal, August, pp. 88-94, 1995.
2. A.M. Okamura, M.L. Turner and M.R. Cutkosky, ”Haptic Exploration of Objects with Rolling and Sliding,” Proc. the 1997 IEEE ICRA, Vol. 3, pp. 2485-2490, 1997.
3. A.M. Okamura, N. Smaby, and M.R. Cutkosky, ”An Overview of Dexterous Manipulation,” Proceedings of the 2000 IEEE International Conference on Robotics and Automation, Symposium on Dexterous Manipulation, Vol. 1, 2000, pp. 255-262, 2000.
4. A. Bicchi, A. Marigo, and D. Prattichizzo, ”Dexterity through rolling: Manipulation of unknown objects,” Proceedings of the 1999 IEEE International Confe
5. P.K. Allen and P. Michelman, ”Acquisition and interpretation of 3-d sensor data from touch,” IEEE Trans. on Robotics and Automation, 6(4), pp. 397-404, 1990.
6. A.M. Okamura, M.A. Costa, M.L. Turner, C. Richard, and M.R. Cutkosky, ”Haptic Surface Exploration,” Experimental Robotics VI, Lecture Notes in Control and Information Sciences, Vol. 250, Springer-Verlag, pp. 423-432, 2000.
7. D.K. Pai, J. Lang, J.E. Lloyd, and R.J. Woodham, ”Acme, a telerobotic active measurement facility,” Experimental Robotics VI, Lecture Notes in Control and Information Sciences, Vol. 250, Springer-Verlag, 2000
8. Yukio Sato and Masaki Otsuki, ”Three-Dimensional Shape Reconstruction by Active Rangefinder,” Proc. 1993 IEEE CVPR, pp. 142-147, 1993.
9. Kengo Nishimura and Hiromi T. Tanaka, ”Active Shape Inferring Based on the Symmetry in Stable Poses,” Proc. the 1996 IEEE ICPR, pp. 136-139, 1996.
10. Hiromi T. Tanaka and Kiyotaka Kushihama, ”Haptic Vision - Vision-based Haptic Exploration,” Proc. the 2002 IEEE ICPR, Vol. 2, pp. 852-855, 2002.
11. Hiromi T. Tanaka and Kayoko Yamasaki, ”Extracting Relational Constraints among Objects with Haptic Vision for Haptic-Interfaced Object Manipulation,” Proc. the 12th ICAT, 2002,
12. Shinichi Tokumoto, Shinichi Hirai, and Hiromi Tanaka, ”Constructing Virtual Rheological Objects,” Proc. World Multiconference on Systemics, Cybernetics and Infomatics, pp.106-111, July, Auland, 2001